Mon. Not. R. Astron. Soc. **000**, 1–15 (1997) Printed 25 July 1997 (MN LaTeX style file v1.4)

Dynamical evolution of rotating stellar systems: I. Pre-collapse, equal mass system

Christian Einsel[1,2] and Rainer Spurzem[2]
[1]*Institut für Astronomie und Astrophysik der Universität Kiel, Olshausenstr. 40, D-24098 Kiel, Fed. Rep. of Germany*
[2]*Astronomisches Rechen-Institut, Mönchhofstr. 12-14, D-69115 Heidelberg, Fed. Rep. of Germany*

Accepted . Received ; in original form

ABSTRACT
The influence of rotation on the dynamical evolution of collisional stellar systems is investigated by solving the orbit-averaged Fokker-Planck equation in (E, J_z)-space. We find that large amounts of initial rotation drive the system into a phase of strong mass loss while it is moderately contracting. The core is rotating even faster than before although angular momentum is transported outwards. At the same time the core is heating. Given these features this phase can be associated with the gravo-gyro 'catastrophe' found by Hachisu (1979). The increase in central angular momentum levels off after about 2-3 initial half-mass relaxation times indicating that the source of this 'catastrophe' is depleted. Finally, the central angular velocity increases again, but with a rather small power of the central density – the same power as for the central velocity dispersion during self-similar contraction towards the collapse. The rotation curves flatten and the ellipticity variations decrease with time, but their shapes are very similar. These results suggest the existence of a self-similar solution for a rotating cluster as well. The maximum values of rotational velocity and ellipticity occur at about the half mass radius.

Key words: methods: numerical – celestial mechanics, stellar dynamics – globular clusters: general.

1 INTRODUCTION

The study of the dynamical behaviour of spherically symmetric, collisional stellar systems has made considerable progress during the last decade. Numerical improvements and refinements are applied to current techniques (Fokker-Planck, Monte-Carlo, fluid-dynamical or N-Body) in order to investigate anisotropy and the post-collapse phase (Bettwieser & Sugimoto 1984, Murphy *et al.* 1990, Heggie & Ramamani 1989, Takahashi 1996a,b, Spurzem 1994, 1996), stochastic energy input due to binaries (Giersz 1996), small-N statistics (Giersz & Heggie 1994ab, Heggie 1996), primordial binaries (Hut 1996), tidal effects, stellar evolution or mass spectra (Chernoff & Weinberg 1990, Lee *et al.* 1991, Fukushige & Heggie 1995, Drukier 1995, Giersz & Heggie 1996, 1997). Considering anisotropy, there are still other features in addition to its hitherto studied effects on the radial variations of density and velocity dispersion, one important effect being the feasibility to flatten those systems. Binney (1978) applied the tensor virial theorem to elliptical galaxies constructed from similar ellipsoids and comprising flat rotation curves, and he derived formulae relating ellipticity to the ratio of rotation velocity and velocity dispersion. The observed spread in v_m/σ for galaxies of a given ellipticity is explained as an effect of anisotropy, which changes the hydrostatic equilibrium.

Observations show that flattening is a common feature of globular clusters, which has been known since the early work done by Pease & Shapley (1917). Measuring projected ellipticities $e = 1 - b/a$ of large globular cluster samples White & Shawl (1987) derive a mean $\bar{e} = 0.07 \pm 0.01$ for 99 clusters in the Milky Way, and Staneva *et al.* (1996) find $\bar{e} = 0.086 \pm 0.038$ for 173 clusters in M31, with maximum values 0.27 and 0.24 of individual globulars, respectively. Kinematical data, i.e. radial velocities of large numbers of cluster members, reveal that this flattening may indeed be explained in terms of rotation, and that the minor axes are nearly coincident with the determined rotation axes (Meylan & Mayor 1986). Dust obscuration, anisotropy or tidal distortion are able to explain individual cases of flattening, but can statistically be ruled out as the main mechanism (White & Shawl 1987).

Significant ellipticity variations are found within globular clusters (e.g., Geyer & Richtler 1981, Geyer *et al.* 1983), and these partly also coincide with the rotation curves obtained by fits to the radial velocity data with some parametrization specified for the velocity field (Meylan & Mayor 1986). Moreover, Kontizas *et al.* (1990) show that the outer parts of globulars in the Small Magellanic Cloud are obviously rounder than the parts inside the half mass radius and it is likely that their structure differs from that of the galactic globular clusters because they are younger (in general) and subject to different tidal forces. The importance of age for the interpretation of observed ellipticities has already been emphasized by Frenk & Fall (1982), who undertook eye-estimates of cluster ellipticities in the Milky Way and the Magellanic Clouds, the latter being slightly larger than the former, which is explained again in terms of internal globular cluster evolution. This view is supported by studies relating Milky Way globular cluster ellipticities to the cluster concentration parameter $c = \log(r_t/r_c)$ (White & Shawl 1987), where r_t is the tidal radius and r_c is the core radius, or to the half mass relaxation time t_{r_h} (Davoust & Prugniel 1990), both representing the dynamical age of a globular cluster. In these two investigations, the average flattening of the dynamically younger systems is significantly larger as well, indicating that loss of angular momentum, presumably originating from diffusion past the escape velocity on relaxation time scales, decreases the ellipticity of a cluster.

Indeed, Agekian (1958) suggested a model in which specific angular momentum is lost due to a relatively large fraction of escaping stars residing in the tail of a rotating Maxwellian velocity distribution shifted towards the direction of rotation as compared to the fraction which is counter-rotating. Considering this effect for every volume element of rotating ellipsoids he obtained a critical ellipticity of $e = 0.74$ below which the systems become rounder with time.

More recently, even larger compilations of radial velocity data have been obtained by different working groups for some globulars. With these data sets they are able to model the velocity field around the core with nonparametric methods, and find in the core of 47 Tuc increasing angular velocities towards the centre (Gebhardt *et al.* 1995), which is interpreted as a gradually faster rotating core due to (gravothermal) contraction of an initially slowly rotating solid body. This would imply that trapping of angular momentum in the contracting core wins over angular momentum transport due to viscosity effects.

Analogously to the discussion whether evaporation or gravothermal contraction drives cluster evolution predominantly, a new question arose due to the stability analysis applied to adiabatically confined, rotating cylinders by Hachisu (1979). He found that, depending on central temperature and angular velocity, there exist cases where, if angular momentum is removed from a shell, gravitational contraction results in an increase in angular velocity, which leads to a runaway in angular momentum transport (by viscosity) and central contraction. In analogy to 'gravothermal catastrophe' this effect is called 'gravo-gyro catastrophe', and the physical origin in the latter case is due to a negative specific moment of inertia, analogously to negative specific heat in the former case. In order to study these effects accurately in a cluster-like structure Akiyama & Sugimoto (1989) set up N-Body simulations for rotating clusters, however, they simulated 1000 particles only. Therefore, the statistical quality of their data is rather poor and consequently, the four-phase evolution proposed by them consisting of *i)* violent relaxation, *ii)* gravo-gyro instability, *iii)* static evolution, *iv)* gravothermal collapse, seems to be rather suggestive than indicative.

Goodman (1983) performed the first numerical simulations solving the orbit-averaged Fokker-Planck equation in (E, J_z)-space applied to rotating stellar systems. His main results are that the difference in ellipticities between old galactic globular clusters and the younger Magellanic clusters can be explained by relaxation processes, though runs representing appropriate cluster structure parameters (e.g., smaller King-W_0-parameters than 9.8) were not stated in his thesis, and that during the self-similar collapse phase the central angular velocity increases as a small power of central density, which is explained by linear perturbation analysis performed on the self-similar solution found by Lynden-Bell and Eggleton (1980). However, this work suffered from coarse numerical resolution and from the problem that determinations of asymptotic values remained open.

A sequence of rotating King models is established by Longaretti & Lagoute (1996), who present an evolutionary path represented by the time evolution of structural parameters; their models take into account evaporation and loss of angular momentum by using simplified expressions and approximations for the derivation of their diffusion coefficients. Some of them emerge to be strong constraints to the general view of evolutionary characteristics of collisional sytems. In particular, deviations from a rotating King form of the distribution function may be significant in advanced stages of cluster evolution.

The present study is aimed to disentangle the effects of evaporation and angular momentum transport stated above and investigating the detailed evolutionary scenarios, when initial models are given, thereby continuing the work begun by Goodman (1983). Moreover, the incorporation of the dynamical effects of rotation is seen as one of the stepping stones towards realistic models of globular clusters; further steps as they have been studied in the non-rotating case (post-collapse, mass spectrum, stellar evolution) are the subject of future papers. A new self-consistent Fokker-Planck solver has been written and is presented together with detailed numerical results. Section 2 gives a description of how the problem is modelled by the Fokker-Planck equation in an axisymmetric coordinate system together with the Poisson equation, while a detailed derivation of the diffusion coefficients is given in the Appendix. Also, possible limitations of the method due to a neglect of the third integral will be discussed. Section 3 provides an overview of the numerical method, and in Section 4 numerical results of the present single mass models are presented. Section 5 summarizes the derived effects of rotation on dynamical evolution, relates it to work from other authors and gives prospects for future work.

2 ORBIT AVERAGED FOKKER-PLANCK EQUATION

2.1 Method

The method described here may be regarded as a continuation of Goodman's (1983) work and the mathematical formulation used here is very near to his, but for the reason that it belongs to a part ("Paper III") of his Ph.D.-thesis, which was never published elsewhere, a description will be repeated here.

In the present study we follow the evolution of the distribution function f as a function of the energy E and the z-component of the angular momentum J_z, both representing velocity variables, with time t. We consider E and J_z as the only isolating integrals and neglect evident non-ergodicity on the hypersurface in phase space given by E and J_z due to any third integral. Because the derivation of the diffusion coefficients necessitates an isolating integral expressed as a function of coordinate space and velocity variables, analytical expansions turn out to be unsuitable for the present technique and J^2 as an approximate third integral in the limiting case of spherical symmetry would be the only choice left to be considered, as it, e.g., has been used in the approximate self consistent dynamical models prepared by Lupton & Gunn (1987). But at the current status of numerical resources we decided to leave the investigations of 3-integral models for the future.

The Boltzmann equation transformed to the new variables then reads as

$$\frac{\partial f}{\partial t} + \frac{\partial \phi}{\partial t}\frac{\partial f}{\partial E} = \left(\frac{\partial f}{\partial t}\right)_{\rm enc} , \tag{1}$$

with the potential ϕ advanced according to the Poisson equation

$$\nabla^2 \phi = 4\pi G n , \tag{2}$$

and the collisional term on the right hand side of Eq. 1, expressed under the Fokker-Planck assumption of small angle scatterings

$$\begin{aligned}\left(\frac{\partial f}{\partial t}\right)_{\rm enc} = \frac{1}{V}\Big(& -\frac{\partial}{\partial E}(< \Delta E > fV) \\ & -\frac{\partial}{\partial J_z}(< \Delta J_z > fV) \\ & +\frac{1}{2}\frac{\partial^2}{\partial E^2}(< (\Delta E)^2 > fV) \\ & +\frac{\partial^2}{\partial E \partial J_z}(< \Delta E \Delta J_z > fV) \\ & +\frac{1}{2}\frac{\partial^2}{\partial J_z^2}(< (\Delta J_z)^2 > fV)\Big) ,\end{aligned} \tag{3}$$

where V is the volume element given by $2\pi/\rho$, with ρ being the radius in cylindrical coordinates. Because the relaxation time t_r is much longer than the dynamical time $t_{\rm dyn}$ of the system, the Boltzmann equation in our problem reduces to an equation in which the distribution function only depends on orbital constants and time. Thus we are allowed to take the orbit average over that area in the meridional plane which intersects with the hypersurface in phase space for which E and J_z are specified. The condition is that kinetic energy in the meridional plane be non-negative:

$$\frac{1}{2}\left(v_\rho^2 + v_z^2\right) \geqq 0 . \tag{4}$$

The volume of this hypersurface is given by

$$p(E, J_z) = 4\pi^2 \int\int_{A(E,J_z)} d\rho\, dz , \tag{5}$$

where the intersection defined by Eq. (4) is given by $A(E, J_z)$, and the factor in front of the integral is due to integration over the third velocity variable, e.g. $\psi = \arctan(v_\rho/v_z)$. Symmetry about the azimuthal direction in coordinate space was assumed.

The orbit averaged Boltzmann equation then takes the form

$$\frac{\partial f}{\partial t} + \frac{1}{p}\frac{\partial q}{\partial t}\frac{\partial f}{\partial E} = \left(\frac{\partial f}{\partial t}\right)_{\rm enc} , \tag{6}$$

in which we introduce the function $q(E, J_z)$ defined to be

$$q(E, J_z) = 2\pi^2 \int\int_{A(E,J_z)} \left(v_\rho^2 + v_z^2\right) d\rho\, dz ; \tag{7}$$

note that the integrand is equal to $2(E-\phi) - (J_z^2/\rho^2)$ and evaluates to zero on the boundary of A. Goodman emphasizes that q is the axially symmetric analogue of the radial action

$$Q(E, J) = 2\int_{r_-}^{r_+} v_r dr \tag{8}$$

in a spherically symmetric potential and comprises actually the average of the radial action over J with boundaries J_z and J_{max}, if the potential is spherically symmetric, thus representing an average of an adiabatic invariant with respect to the third integral.

Interpreting $q(E, J_z)$ as an adiabatic invariant itself, equation 6 indicates that, neglecting any encounters,

$$\left.\frac{\partial f}{\partial t}\right|_{q,J_z} = 0 , \tag{9}$$

from which it follows, that there is a redistribution of energies in the system, but the 'adiabatic invariant' q and the angular momentum are conserved. The desired solution of the Boltzmann equation therefore may be split into two parts: the first is to calculate the evolution due to stellar collisions (i.e. small angle scatterings: the Fokker-Planck step) with the potential held fixed and the second is to advance the distribution function f due to slow adiabatic changes in the potential with $f(q, J_z) = const.$

The Fokker-Planck equation is transformed into flux conservation form in order to improve conservation of several quantities:

$$\frac{df}{dt} = \frac{1}{p}\left(-\frac{\partial F_E}{\partial E} - \frac{\partial F_{J_z}}{\partial J_z}\right) \tag{10}$$

with particle flux components

$$F_E = -D_{EE}\frac{\partial f}{\partial E} - D_{EJ_z}\frac{\partial f}{\partial J_z} - D_E f \tag{11}$$

$$F_{J_z} = -D_{J_zJ_z}\frac{\partial f}{\partial J_z} - D_{J_zE}\frac{\partial f}{\partial E} - D_{J_z} f . \tag{12}$$

The orbit averaged flux coefficients D_{ii} in these equations are derived from the local diffusion coefficients, which again are found for the axial symmetric geometry via the prescriptions of Rosenbluth *et al.* (1957) involving covariant derivatives instead of the procedure employed by Goodman (1983) using a non-covariant form. The derivation of the flux coefficients is given in the Appendix. Comparison of the expressions for the diffusion coefficients found by us and Goodman reveals complete agreement.

The derivation of the diffusion coefficients makes it necessary to specify a background distribution function by which test stars are scattered. Using self-consistently the foreground distribution for the background would require computational time proportional to $N_\rho \times N_z \times N_E^2 \times N_{J_z}^2$, where the N_i are grid sizes in coordinate and velocity space, which would reduce the grids employed to inaccurate descriptions of the current problem; thus, as in all previous applications concerning 2D Fokker-Planck methods for stellar systems, we set up an appropriate form of the background distribution. Herein we follow Goodman (1983) giving a rotating Maxwellian velocity distribution to the background,

$$f_b(\vec{v}) = \frac{\rho}{(2\pi\sigma^2)^{\frac{3}{2}}} \exp(-\frac{(\vec{v}-\Omega\rho\vec{e}_\varphi)^2}{2\sigma^2}) \tag{13}$$

where ρ, Ω and σ correspond to the zeroth, first and second order moments of the distribution function, and are the density, angular velocity and one-dimensional velocity dispersion of the field star distribution, respectively. Applying this form (Eq. (13)) to the background distribution yields analytical expressions in the diffusion coefficients parametrized locally by the three moments mentioned above, just thereby reducing the computational efforts necessary.

2.2 Initial conditions

For starting configurations rotating King models are utilized. These are of the form

$$f_{rk}(E, J_z) = \mathrm{const} \cdot (e^{-\beta E} - 1) \cdot e^{-\beta\Omega_0 J_z} , \tag{14}$$

where $\beta = 1/(m\sigma_c^2)$ and the dimensionless angular velocity $\omega_0 = \sqrt{9/4\pi G\rho_c} \cdot \Omega_0$ are parameters to be specified for each model. In order to construct a potential-density pair, β is related to the King-parameter (dimensionless potential) $W_0 = -\beta m(\phi - \phi_t)$. Throughout this paper our different evolutionary runs are parametrized uniquely by the set of initial conditions given by its respective pair (W_0, ω_0). In establishing the starting models we follow Lupton & Gunn (1987) and take advantage of an almost always converging iteration procedure between evaluation of the potential, brought into the form of a multipole expansion, and the determination of the density, where different types of Gauss-integrations are performed and thereby slightly different numerical procedures are employed (Einsel & Spurzem 1994).

For simplicity and scaling reasons we choose the gravitational constant G, the initial cluster mass M_i and the initial core radius r_{c_i} to be one, i.e. to be our system units. The unit of time is expressed as (Cohn 1979)

$$t_0 = \sqrt{\frac{r_{c_i}^3}{GM}} \cdot \frac{(GM)^2}{4\pi\Gamma}\frac{1}{N} , \tag{15}$$

$\Gamma = 4\pi(Gm)^2 \ln\Lambda$, where N is the total number of particles, $\ln\Lambda$ is the coulomb logarithm and m is the mean mass of particles (equal to $1/N$ in the present single mass models). The first factor on the right hand side is simply the dynamical time of the system and evaluates to one with the units given above, while the second factor scales out with factors standing in front of the diffusion coefficients simplifying their expressions appreciably, then. An expression for the initial half mass relaxation time is taken from Spitzer & Hart (1971)

$$t_{r_h,i} = 0.138\sqrt{\frac{N \cdot r_{h_i}^3}{G \cdot m}}\frac{1}{\ln\Lambda} \tag{16}$$

$$= 32.5 , \tag{17}$$

in units of t_0 (Eq. (15)), and we assume $\Lambda = 0.4 \cdot N$. Due to mass loss the relaxation time may change by a factor of 2-4 during the runs presented here.

3 NUMERICAL METHOD

3.1 Computational grid

In order to obtain an appropriate grid representation, e.g. a sufficiently resolved core and rectangular grid, a transformation of the basic variables was performed. Following Cohn (1979) we take

$$X(E) = -\ln\left(\frac{E}{2\phi_c - E_0 - E}\right) , \tag{18}$$

where E_0 is the energy of a circular orbit at the core radius of the cluster. Thus, inside the core (roughly $\phi_c \leqq E \leqq E_0$) the relation is nearly linear, while the proportionality $X \propto -\ln|E|$ in the halo improves the spacing of the radii of circular orbits with given energies in the direction of the tidal boundary. For any specified energy the z-component of the angular momentum is normalized to the maximum angular momentum for that energy, which again is the angular momentum of the corresponding circular orbit as a function of E:

$$Y(J_z, E) = \frac{J_z}{J_{z,0}(E)} , \tag{19}$$

For each time step $r_{circ}(E)$ and $J_{z,0}(E)$ are determined from the evolving potential in the equatorial plane by a simple Newton-Raphson scheme. At the same time the central potential changes, so that the complete (X, Y)-grid is adapted to the new situation.

3.2 Fokker-Planck step

A finite difference scheme is used to integrate the diffusion part of the problem and the discretized equation system is solved implicitly with the help of a sparse matrix method (Henyey 1959) borrowed from a gaseous model code (Spurzem 1994, 1996). A Chang-Cooper scheme is applied to the energy direction in order to improve conservation characteristics (Chang & Cooper 1970).

A double-logarithmic coordinate space grid is constructed for the meridional plane (ρ, z), which extends initially from 10^{-3} core radii to somewhat beyond the tidal radius. During all runs described here it was adjusted to the contracting core radius $r_c(t)$ by the condition $\rho_{i=0} = z_{i=0} = 0.001 \cdot r_c(t)$ for the innermost grid point. This was usually done only about 4-6 times in each run in order to avoid rounding errors due to the necessary interpolation procedure involved.

Because of deviations of the local velocity distribution from a rotating Maxwellian (Eq. (13)) especially in the outer halo, energy and angular momentum are not sufficiently conserved if the local foreground values of angular velocity and velocity dispersion are provided as parameters for the background distribution function. Instead, these were used as starting values for an iteration procedure which determines new, consistent background values for ω and σ under the condition that integrals of f_b times the local first order diffusion coefficients $< \Delta E >$ and $< \Delta J_z >$ (given in the

Appendix) over velocity space are zero (Goodman 1983), expressing the fact that locally no energy and angular momentum may be generated or removed just by diffusion.

3.3 Vlasov step

After diffusion has taken place for an appropriate amount of time, the potential has to be advanced. The density is calculated from the distribution function according to

$$n(\rho, z) = \frac{2\pi}{\rho} \int\limits_{\phi_c}^{E_{\rm tid}} \int\limits_{-\rho\sqrt{2E-2\phi}}^{\rho\sqrt{2E-2\phi}} f(E, J_z) dE dJ_z \,. \qquad (20)$$

Given this density distribution, Eq. (2) can be solved to obtain the potential. A multipole expansion is carried out to determine Dirichlet boundary values of ϕ beyond the tidal radius in the meridional plane. Symmetry is assumed about the equatorial plane so that v. Neumann boundary conditions

$$\left.\frac{\partial\phi}{\partial z}\right|_{z=0} = 0 \,, \; \left.\frac{\partial\phi}{\partial\rho}\right|_{\rho=0} = 0 \qquad (21)$$

are applied at the inner boundaries. The system of equations is solved with the same sparse matrix method (Henyey *et al.* 1959) as for the diffusion step, thereby taking account of the even sparser matrices occurring due to the Poisson equation.

Having built the potential a new (E, J_z)-grid is created, the meridional plane is scanned to determine the area $A(E, J_z)$ and Eq. (7) is numerically integrated to obtain the adiabatic invariant q. It is required in order to fulfil the conservation of $f(q, J_z)$. At first, the new (E, J_z)-grid is transformed uniquely into a (q, J_z)-grid. A second order bivariate Taylor expansion is then performed for each mesh point in the new grid to derive approximate values from the known values of $f(q', J_z')$ in the old grid. I.e., $f(E, J_z)$ is allowed to change. This again gives a new density distribution ρ in Eq. (20) and the procedure is repeated until convergence is reached. In doing this the firstly determined $f(q, J_z)$ is retained as the old grid in order to save accuracy. Nevertheless, this second order interpolation step turns out to be the relatively most important source of numerical error in the code.

Goodman (1983) reports a test of the influence of the third integral on the procedure just stated. He relaxed an initial King model distribution function (non-rotating) violently in assigning to it a Plummer potential. The result was a strong dynamical collapse with an increase in ρ_c of a factor of 56. The collapse generated a flattening $e = 0.055$, which is attributed to the third integral, because there is no preferential axis of rotation or anisotropy initially, that could flatten the system. On the other hand, the test is very crude, because as Goodman himself states the above procedure is just first order in energy conservation between initial and final values of ϕ and the collapse picture is not appropriate to be described by adiabatic invariants. Though the effect of diffusion is to wipe out the (here artificially) generated azimuthal anisotropy, we consider the flattening of nonrotating, isotropic configurations during their evolution as a more appropriate measure of the influence of the third integral.

3.4 Computation and conservation characteristics

The evolution of the system is followed numerically with time steps Δt chosen to be proportional to the central relaxation time t_{r_c} starting with $\Delta t = 0.125\, t_{r_c}$ e.g. in case of a model with $W_0 = 6$, but the coefficient was increased from time to time by a factor of $\frac{4}{3}$ in order to have a fractional increase of the central density between 3−6%. In analogy with the computations done by Cohn (1979) these runs ended with coefficients of about 2. Inbetween one Vlasov step, i.e. one recomputation of the potential, four Fokker-Planck steps, i.e. diffusion steps, were carried out.

In order to stay as close to the King-model distribution functions as possible we set up a strict tidal cutoff. The tidal boundary is adjusted so as to ensure that the mean cluster density is conserved throughout the evolution (see, e.g., Spitzer 1987). The fluxes at the $Y = \pm 1$-boundaries are set to zero as well as at the $E = \phi_c$-boundary. The only open boundary then is the $E = E_{\rm tid}$-boundary, where the condition $f(E_{\rm tid}, J_z) = 0$ was fixed. The first derivative of f with respect to E is non-zero at the boundary and is evaluated just inside the boundary in order to obtain accurate escape fluxes. With grid sizes of $N_X = 100, N_Y = 61, N_\rho = N_z = 80$ used here the errors in mass, energy and angular momentum all accumulated to about 0.4%, 0.7% and 1.7% respectively for a typical model by the time the central density increased by about 5-6 orders of magnitude, when the runs were stopped. Goodman obtained errors 7.9% (12.7%) in mass, 6.5% (2.9%) in energy and 16.5% (24.1%) in angular momentum for runs with $N_X = 40, N_Y = 10$ ($N_X = 20, N_Y = 10$) extending over $2\frac{1}{2}$ orders of magnitude, while Cohn (1979) reports an error in mass of only 0.04%, which may easily be explained by the application of spherical symmetry to real space in his simulations.

Typical runs for the evolution of one model up to a density increase of 5 orders of magnitude needed about 60 hours on a 100 Mhz hyperSPARC workstation (Maths Dept. in Edinburgh University) or 150 hours on a 40 Mhz SPARCstation (University of Kiel), respectively. Using a parallelized version of the code (message passing) on a CRAY T3D 40 hours were needed, when 8 processors were utilized. Although this speedup is not yet convincing, parallel processing is highly recommended for multi-mass versions of the present code.

Although simulations with several choices of W_0 have been carried out, the results presented here concentrate on those runs with $W_0 = 6$ leaving the results with different W_0 to the summary section and/or subsequent papers. Additional features indicated by those do not restrict or alter the conclusions drawn by using just the results from $W_0 = 6$. The initial conditions of all models with $W_0 = 6$ are summarized in Table 1. Given are the rotation parameter ω_0, the ratio of rotational to total kinetic energy, the dynamical ellipticity (*cf.* Eq. (26)), the ratios of tidal and half-mass radii to initial core radii, the central and finally the half-mass relaxation time in system units.

4 NUMERICAL RESULTS

4.1 Evolution of cluster structure

The evolution of Lagrangian radii with time for models with $W_0 = 6.0$ and $\omega_0 = 0.0, 0.5, 1.0$ is shown in Figure 1. In

Table 1. Initial conditions of all models presented with $W_0 = 6$.

ω_0	$T_{\rm rot}/T_{\rm kin}$	$e_{\rm dyn}(0)$	$r_{\rm tid}/r_{\rm c}(0)$	$r_{\rm h}/r_{\rm c}(0)$	$\tau_{\rm rc}(0)$	$\tau_{\rm rh}(0)$
0.00	0.00	-0.001	18.72	2.70	19.24	91.88
0.05	0.23	0.002	18.61	2.70	19.23	91.77
0.10	0.89	0.013	18.25	2.68	19.22	90.80
0.20	3.38	0.051	16.83	2.66	19.20	89.71
0.30	7.00	0.105	14.99	2.62	19.21	87.73
0.40	11.23	0.165	13.08	2.55	19.22	84.12
0.50	15.61	0.224	11.46	2.48	19.27	80.49
0.60	19.81	0.278	9.94	2.39	19.40	76.32
0.70	23.71	0.327	8.77	2.30	19.50	71.78
0.80	27.18	0.368	7.69	2.20	19.71	67.37
0.90	30.25	0.403	6.88	2.12	19.86	63.24
1.00	32.99	0.433	6.22	2.04	20.02	59.63

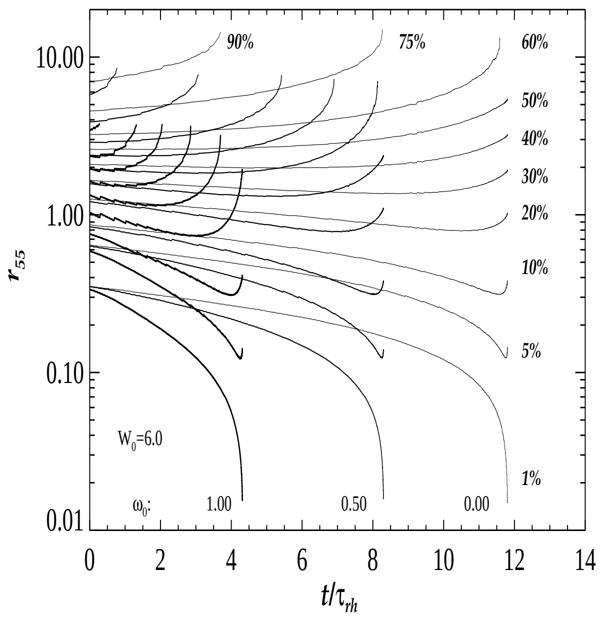

Figure 1. Evolution of mass shells (Lagrange radii r_{55}) for the model $(W_0, \omega_0) = (6.0, 0.60)$. Shown are the radii for mass columns containing the indicated percentage of total mass in the direction of the $\theta = 54.74°$-angle.

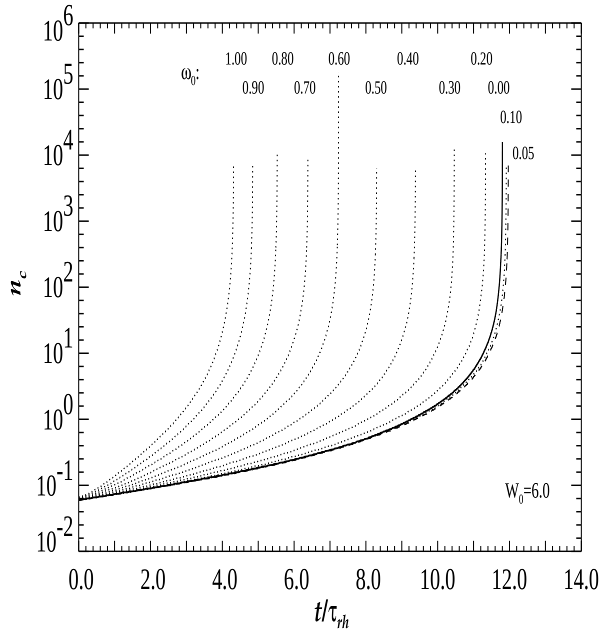

Figure 2. Comparison of central density evolution for models with same $W_0 = 6.0$, but different initial angular velocity parameter $\omega_0 = 0.0...1.0$. The time is given in units of initial half mass relaxation times $t_{r_h,i}$.

flattened systems the definition of Lagrangian radii is not straightforward. Just only for that purpose we assume here, since flattening is small, that deviations from spherical symmetry are only up to second order in a Legendre expansion. Thus, we evaluate the Lagrange radii at a zenithal angle, where the effects of a probable flattening on the mass columns are expected to be less important: $P_2(\cos\theta) = 0$, which gives $\theta = 54.74°$. Thereby, we determine $\rho(r, \theta)$ and then compute

$$M(r) = \int_0^r 4\pi\rho(r, 54.74°)r^2 dr \; . \tag{22}$$

The tidal radius is determined from the condition $\phi(\rho, z) = E_{\rm tid}$ and is obtained here for the same angle as described above.

The overall structure of evolution of mass shells closely follows what was given by previous non-rotating, isotropic or anisotropic models (e.g. Aarseth, Hénon & Wielen 1974, Cohn 1979, Giersz & Heggie 1994a,b, Giersz & Spurzem 1994) disregarding the existence of and evaporation through the tidal boundary. An expansion of mass shells larger than 50% is observed and an initially smooth – later accelerated – contraction of the inner mass shells can be seen. The core radius decreases appreciably as well as the core mass. While no special sign of a gravo-gyro contraction (i.e. contraction, levelling off and (gravothermal) contraction again) is detectable, strong mass loss is evident in this diagram through the loss of complete mass shells. The tidal radius, which is not shown directly in the diagram, decreases in order to maintain the condition that the mean density in the cluster orbiting around a parent galaxy is conserved.

Figure 2 shows a comparison of the density evolution of a sequence of models with the same initial $W_0 = 6.0$ but with different $\omega_0 = 0.0...1.0$, respectively. The non-rotating model reaches singularity in its core after about $t_{cc} \approx 11.81 t_{r_h,0}$. This has to be compared with previously derived collapse

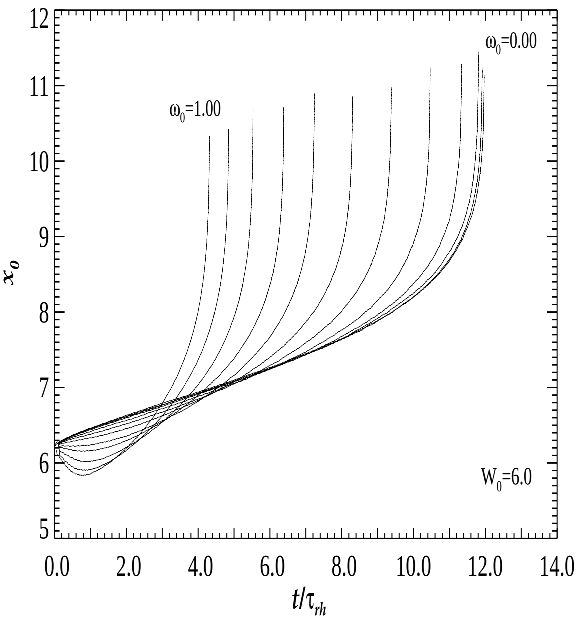

Figure 3. Comparison of scaled escape energy evolution for models with same $W_0 = 6.0$, but different initial angular velocity parameter $\omega_0 = 0.0...1.0$. The time is again given in units of initial half mass relaxation times $t_{r_h,i}$.

time scales, which were in many cases determined for isolated Plummer models, giving $t_{cc} \approx 15.5...17.6\, t_{r_h,0}$ (Cohn 1979, 1980, Takahashi 1996ab). Chernoff & Weinberg (1990) find times to reach core collapse for isolated King models (without stellar evolution) with initial value $W_0 = 3.0$ ($W_0 = 7.0$, $W_0 = 9.0$) of $t_{cc} = 9.6\, t_{r_h,0}$ ($t_{cc} = 10.1\, t_{r_h,0}$, $t_{cc} = 2.23\, t_{r_h,0}$, respectively). Note that the latter two values were not published in their paper, but reported by Quinlan (1996), who himself finds a collapse time for the corresponding isotropic ($f(E)$) King model (case of $W_0 = 6.0$) with tidal mass loss to be $t_{cc} = 12.9\, t_{r_h,0}$. Detailed comparison with Quinlan's sequence of King models from $W_0 = 1$ up to $W_0 = 12$ reveals a systematic difference of about 10 % between our and his results. An increase of the numerical resolution, i.e. the grid sizes, in the present models results in slightly larger collapse times thereby approaching Quinlan's accurate values. Regarding the partly large differences between collapse times determined with distinct methods for (nearly) the same problems (isotropic or anisotropic models) reported in the literature, we conclude that our results for the non-rotating models may be considered as to be in close agreement with previous work on that field.

On the other hand Fig. 2 gives accurate information about the influence of rotation on collapse time. The strongest rotating model with $\omega = 1.0$ gives the smallest $t_{cc} = 4.3 t_{r_h,0}$, implying that rotation accelerates the collapse. While there is no three- or four-phase structure of contraction or collapse phases of different origin (Akiyama & Sugimoto 1989), the steeper slope in central density in the higher rotation case indicates the existence of a gravo-gyro contraction, which then transforms into gravothermal collapse which is more advanced than in the non-rotating case.

A similar picture derives from Figure 3, where the time evolution of the scaled escape energy

$$x_0 = \frac{(\phi_t - \phi_c)}{\sigma_c^2} \tag{23}$$

(σ_c is the one dimensional central velocity dispersion) is shown. It is noteworthy that all models show the steep upturn in x_0, when they approach the collapse time and they arrive at values of x_0 between 8.0 and 9.0. This feature (and with this range of values) has already been described theoretically by Lynden-Bell & Wood (1968) and numerically by Cohn (1979), so that we are in agreement with previous results interpreting this in terms of gravothermal instability. The effect of rotation can be seen in the earlier evolution: the model with $\omega = 1.0$ is prevented from the usual deepening of the potential scaled by the velocity dispersion in the centre of the cluster and stagnates near its starting value of x_0. Considering the stronger increase in central density inferred from Figure 2 for this model at the same time, the reason for the behaviour in Fig. 3 will be found in a relatively strong increase in the central velocity dispersion. The sources of this effect then subside slowly and a smooth turnover into the fast collapse is traced, and so this model crosses the paths of the still gently contracting slow- and non-rotating configurations.

To clarify these processes we plot in Figure 4 the central velocity dispersion against central density. The evolution starts in the lower left corner of the diagram. While the slowly and non-rotating models show the typical sign of an initial reluctance to increase in velocity dispersion as is the case for isotropic and anisotropic systems (e.g. Cohn 1979), the rapidly rotating model ($\omega_0 = 1.0$) seems to suffer a significant thermalization and heating of its core. The evolutionary paths then join again and start the self-similar collapse phase, which is characterized by the quantity

$$\gamma = \frac{d \ln \sigma_c^2}{d \ln \rho_c}\,, \tag{24}$$

which represents twice the slope in the double logarithmic plot (σ_c, not σ_c^2 is plotted). From all models of our 2D-calculations we derive an average $\gamma = 0.109$ with no dependence of γ on the amount of initial rotation, implying that initial rotation seems to have a minor influence on collapse characteristics. Cohn's (1979) and Takahashi's (1996a) 2D-results show $\gamma = 0.12$ and 0.10, respectively, and Cohn (1980) obtains $\gamma = 0.10$ from his isotropic systems in rough agreement with our result. Goodman (1983) also derives a value of 0.10 for γ with his low resolution grids.

The gravo-gyro picture by Hachisu (1979) indicates that the positive variation of temperature in the core is due to a rise in entropy caused by viscosity effects, when angular momentum is transferred to disordered motion, and is thereby effectively carried outwards (negative specific moment of inertia). In Fig. 5, a plot of central angular velocity versus central density is given in the same manner as the $\log(\sigma_c) - \log(\rho_c)$ diagram above, but only for the rotating models. There is a pronounced initial increase in angular velocity for the most rapidly rotating model, which after about 2.5 $t_{r_h,i}$ reaches a plateau and finally turns over into a power law relation of constant slope in this logarithmically plotted diagram when roughly 4 $t_{r_h,i}$ have passed by. The

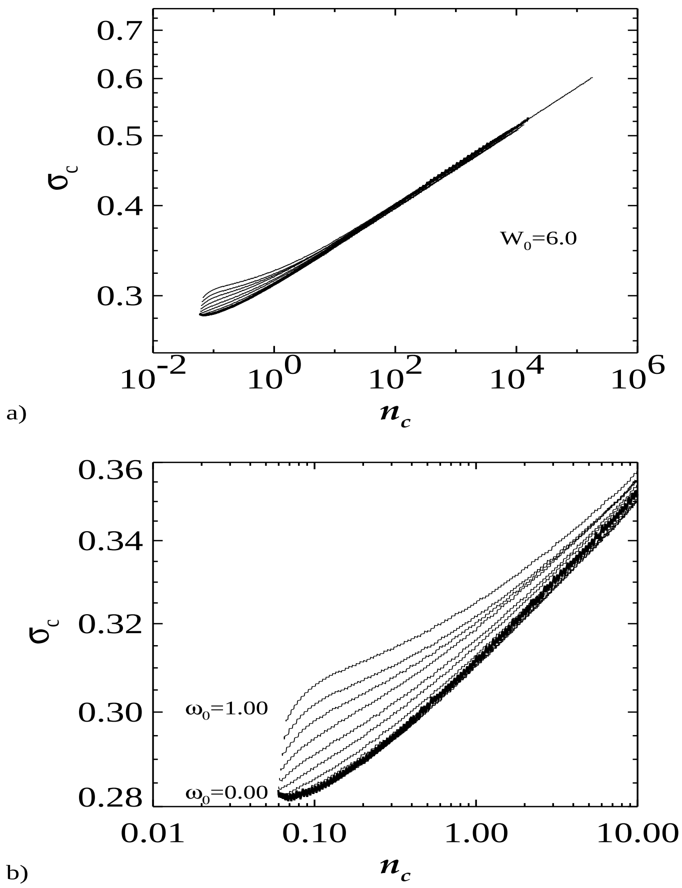

Figure 4. Evolution of central velocity dispersion versus central density for the same models as in Figure 3. The curve of the stronger rotating models show a remarkable upturn at the beginning (i.e. at low densities).

increase in ω_c is connected with the heating process evident from Figure 4.

The stagnation phase after the initial increase marks the time, when most of the total angular momentum is diminished (transported into the outer halo or evaporated) ending the state of negative specific moment of inertia in the core. The further evolution is now determined by self-similar evolution in the gravothermal picture, as can be seen if we take a rough measure of the quantity

$$\delta = \frac{d \ln \omega_c}{d \ln \rho_c} . \tag{25}$$

Inspection of Figure 5 reveals $\delta = 0.06...0.08$ (with a small dependence on the amount of initial rotation), which means, that azimuthal (rotational) velocities in the decreasing core increase in roughly the same way as any other velocity (inferred from $\gamma/2 \approx 0.055$). Goodman found values $\delta = 0.14$ for grid size $(N_X \times N_Y) = (20 \times 10)$ and $\delta = 0.10$ for a (40×10)-grid.

Several useful quantities derived from the models presented here are shown in Tab. 2. In column (1) the initial angular velocity in system units is given ($W_0 = 6$), col. (2) gives the collapse time, col. (3) the collapse rate, col. (4) the number of current central relaxation times, $\tau_{\rm rem}$, until complete collapse in the self-similar evolution phase, col. (5)

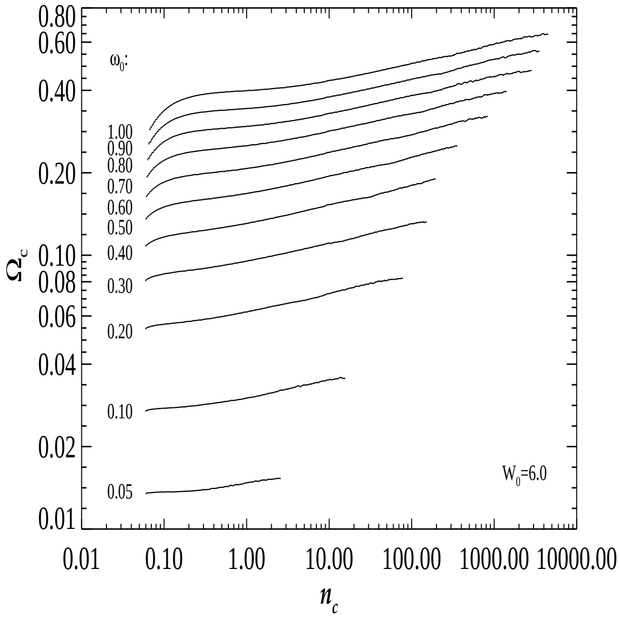

Figure 5. Evolution of angular momentum versus central density for all rotating models with $W_0 = 6.0$.

Table 2. collapse parameters of all simulated models with $W_0 = 6$.

ω_0	$\tau_{\rm cc}$	ξ	$\tau_{\rm rem}$	γ	δ	$\frac{\Delta M}{\tau_{\rm rh}(0)}$	$\frac{\Delta J_z}{\tau_{\rm rh}(0)}$
0.00	11.804	4.69	256	0.111	–	2.2	–
0.05	11.967	5.04	239	0.113	0.045	2.2	6.3
0.10	11.913	4.82	247	0.107	0.071	2.3	7.1
0.20	11.334	4.61	261	0.112	0.079	2.9	8.7
0.30	10.463	4.74	251	0.106	0.077	4.0	11.6
0.40	9.383	4.79	249	0.108	0.075	5.5	16.0
0.50	8.302	5.03	240	0.114	0.074	7.3	21.4
0.60	7.238	4.53	263	0.107	0.066	11.4	32.3
0.70	6.387	4.84	245	0.111	0.068	14.1	39.2
0.80	5.532	4.70	252	0.104	0.061	20.4	56.7
0.90	4.850	5.04	237	0.109	0.066	24.5	71.1
1.00	4.318	4.89	244	0.108	0.065	29.9	92.5

and (6) the exponents used in the corresponding equations of state of the core, while col. (7) and (8) state the percentage of initial mass and angular momentum loss per half mass relaxation time. Note, that the non-rotating model gives mass loss rates in full agreement with those reported in the literature (e.g. Spitzer 1987), with strongly increasing values towards models of higher rotation. Unfortunately, the well known value of 320 for $\tau_{\rm rem}$ (Cohn 1980) is underestimated by our models, which indicates that these suffer from worsening numerical resolution, when the collapse proceeds further and further.

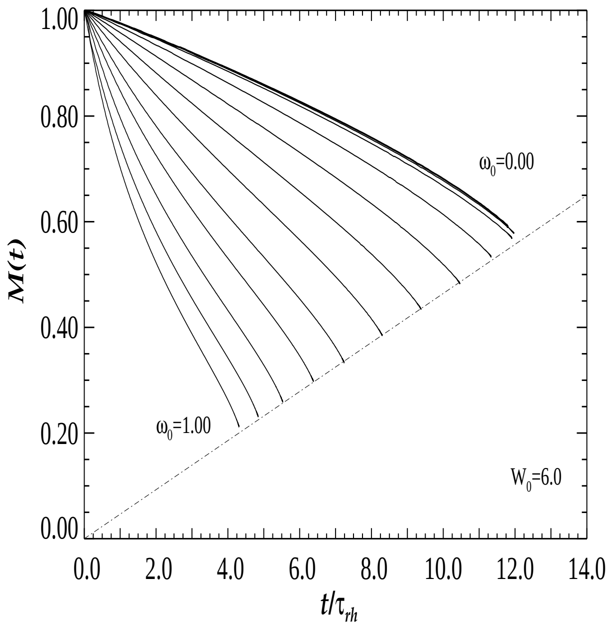

Figure 6. Evolution of total mass retained in the cluster models with $W_0 = 6.0$.

4.2 Evolution of cluster shapes

As has already been shown in Figure 1, our models – subject to the strict tidal boundary formulation given above – suffer strong mass loss, which can also be seen from Figure 6. Here, a comparison of preserved mass as a function of time between the models with same $W_0 = 6.0$ but different rotation ($\omega_{0,i} = 0.0...1.0$) is given. In general this diagram reveals information about evaporation of angular momentum from the halo, which drives cluster evolution with respect to rotation. As expected the fastest rotating model shows strongest mass loss indicated by the slope of the curves, and within its evolution an even steeper mass loss can be found in the initial two half mass relaxation times, which were associated with the gravogyro phase of the system.

By transforming formulae derived by Binney (1978), who applies the tensor-virial theorem to a system composed of similarly situated ellipsoids, Goodman (1983) defines the so-called dynamical ellipticity $e_{\rm dyn}$, which then is given by

$$\frac{2T_{rot} + 3T_{\sigma_\phi} - T_\sigma}{T_\sigma - T_{\sigma_\phi}} = \frac{(1+2s^2)\arccos s \; - \; 3s\sqrt{1-s^2}}{s\sqrt{1-s^2} \; - \; s^2 \arccos s}\,, \quad (26)$$

where $s \equiv b/a = 1 - e_{\rm dyn}$ is the axis ratio of the ellipsoids, which are assumed to be oblate spheroids (i.e. not triaxial), T_{rot} is the rotational energy, T_{σ_ϕ} is the energy contained in the azimuthal component of the velocity dispersion and T_σ is the energy associated with all components of the velocity dispersion. For sufficiently small $e_{\rm dyn}$ this relation may be expressed as

$$\frac{2T_{rot} + 3T_{\sigma_\phi} - T_\sigma}{T_\sigma - T_{\sigma_\phi}} \approx \frac{8}{5} e_{\rm dyn}\,. \quad (27)$$

The evolution with time of $e_{\rm dyn}$ (calculated from Eq. (26)) is plotted in Figure 7 for the three models with $W_0 = 6.0$. A steep decrease in ellipticity can be seen for the initially most strongly rotating model and the final states of all models lack significant flattening. Due to less effective mass loss, the angular momentum transport beyond the tidal boundary is smaller in the more moderately rotating models, so that the respective curves are able to cross each other.

Spherical symmetry is not exactly preserved for the non-rotating model (see Fig. 7, curve $\omega_0 = 0$), which can be explained by the creation of anisotropy in its halo, when azimuthal pressure is compared with that within the meridional plane. Because there is a preferential direction due to the chosen coordinate system, i. e. the z-direction, no anisotropy may develop in planes tangential to the poles of the system. Thus, just as radial anisotropy develops in general spherical systems (e.g., Cohn 1979, Louis & Spurzem 1991), it evolves in the equatorial plane of our model configurations, but not along the z-axis with $\rho \ll r_c$, which is caused by the neglect of the third integral. Moreover the present formulation of the tidal boundary produces an anisotropy profile, which shows the usual rise towards the halo starting from the isotropic core, but then, as it approaches the tidal boundary, falls below zero, because stars on radial orbits are evaporated more effectively than stars on tangential orbits: the former easily gain energy in core passages, so that those orbits are deplenished. On the other side stars visiting regions near the poles are all coupled to the core, because no third integral specified prevents them from doing that (e.g., J^2 in the spherical symmetric case, if it is non-zero for the orbit given).

Neglect of the third integral also has effects on orbits when slow potential changes take place. Consider circular orbits in the meridional plane and equatorial plane and assume a currently spherical potential. A gentle contraction of the system will retain a circular orbit in the equatorial plane, since it is represented accurately by its (E, J_z)-pair (it will just be shifted to that energy, where $J_{z,0}(E) = J_z^{old}$ for angular momentum has to be conserved), while the former orbit is not distinguished by our coordinate systems from radial orbits of the same energy. Therefore, all orbits with $J_z = 0$ are shifted to new energies (via the condition of adiabatic invariant conservation) corresponding to the ensemble mean with respect to third integral, and this may not be the same energy in the meridional circular orbit case as that of the equatorial circular orbit. In particular, the probability of retaining a circular orbit is not necessarily one.

Nonetheless, inspection of Figure 7 indicates, that the ellipticity of the non-rotating model rises due to the neglect of the third integral only to values $e_{\rm dyn} \approx 0.01$, well below the uncertainties inferred from observations.

In Figure 8 the variation of unprojected ellipticities $e = 1 - b/a$ with radius is shown for the model with $\omega_0 = 0.50$ for several evolutionary times. The current core radii are indicated by triangles on the curves, respectively. The ellipticities of the core are evidently smaller as is the case already for the starting models. The ellipticity peaks at about the half mass radius where it is appreciably larger than in the core but with a nearly constant offset ($\Delta e \approx 0.07$ in this case). This indicates, that we indeed expect a significant ellipticity variation within globular clusters as has been stated by Geyer *et al.* (1983). It is remarkable that the contraction or decrease of the core is not reflected in this picture. The horizontal lines in this Figure give for comparison the respective dynamical ellipticities $e_{\rm dyn}$ for that time step. It

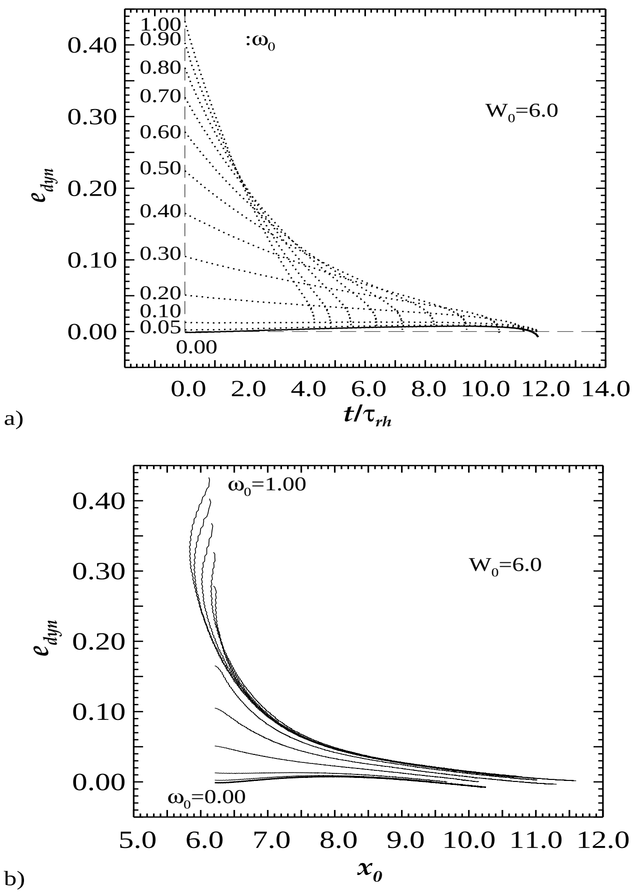

Figure 7. Evolution of dynamical ellipticity $e_{\rm dyn}$ as defined by Goodman (1983) (Eq. (27) see text for explanation) for all models with $W_0 = 6.0$. Fig. a) gives the evolution versus time measured in units of the half mass relaxation time, while Fig. b) shows the evolution versus the scaled escape energy x_0.

seems, that this quantity represents very well a global mean unprojected ellipticity.

Strong evidence for rotation in globular clusters had been derived from the observed coincidence of ellipticity and rotational velocity profiles, both being scaled arbitrarily (Meylan & Mayor, 1986). In Figure 9 we show for comparison for the same model and time steps as in Fig. 8 the corresponding profiles of rotational velocity. Prior to gravothermal instability a coincidence of the profiles just stated may indeed be watched, while for the rotational velocity curve corresponding to the gravothermal collapse phase

Recently, maps of rotational velocities and azimuthal as well as meridional velocity dispersions have been constructed from non-parametric fitting of large samples of kinematical data for ω Cen (Merritt *et al.* 1997). Disregarding for the moment the simplicity of the present models (i.e. single mass models, no stellar evolution, etc.) we chose a model from our simulations, which roughly reproduces the ellipticity and concentration parameter (0.12 and 1.36, respectively) derived for ω Cen from observations. The velocity maps obtained ($W_0 = 6$, $\omega_0 = 0.6$, $t = 3.77\ \tau_{rh_0}$) are shown in Fig. 10. These maps agree with those from Merritt *et al.* (1997) in the morphological structure, e.g. the oblate isovelocity contours in the case of σ_ϕ or the torus-like con-

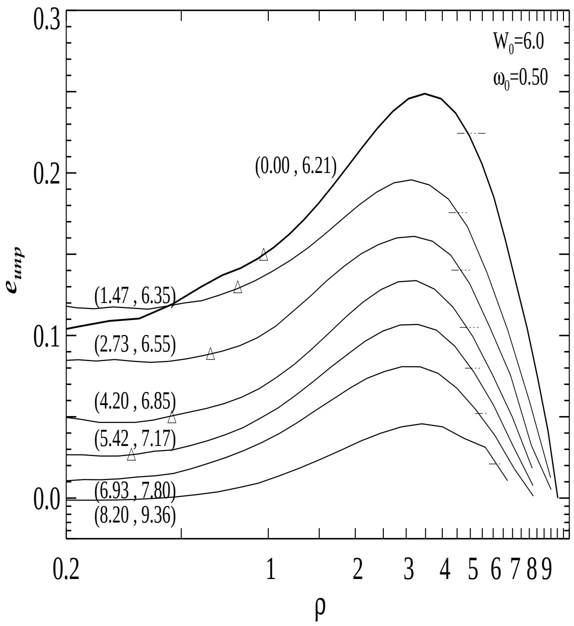

Figure 8. profile of unprojected ellipticity for model with $W_0 = 6.0$ and $\omega_0 = 0.50$ for several evolutionary times as indicated. The pairs in brackets give x_0 and $t/t_{\rm rh}$, respectively. The horizontal lines on the right side indicate the corresponding dynamical ellipticities.

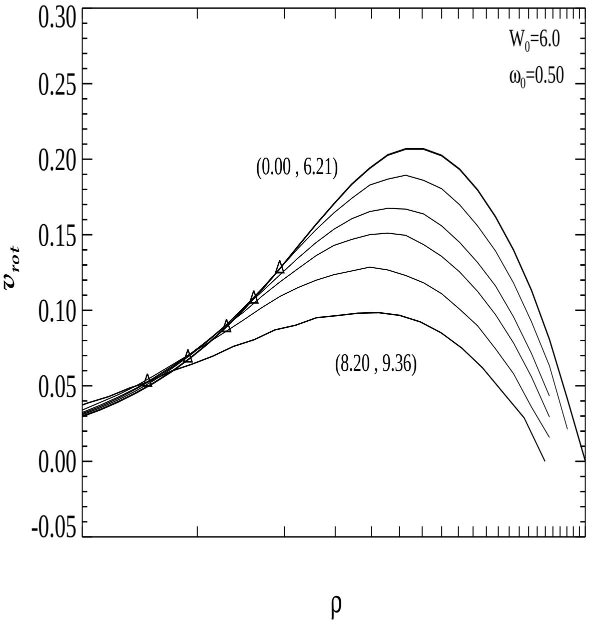

Figure 9. profile of rotational velocities $v_{\rm rot}$ for model with $W_0 = 6.0$ and $\omega_0 = 0.50$ for several evolutionary times as indicated. The pairs in brackets give x_0 and $t/t_{\rm rh}$, respectively. The sequence of curves starts with the pair $(0.00, 6.21)$ at the top. The actual core radii are denoted by the triangles put on the curves, respectively. The core radius of the last model plotted is situated left from the figure area.

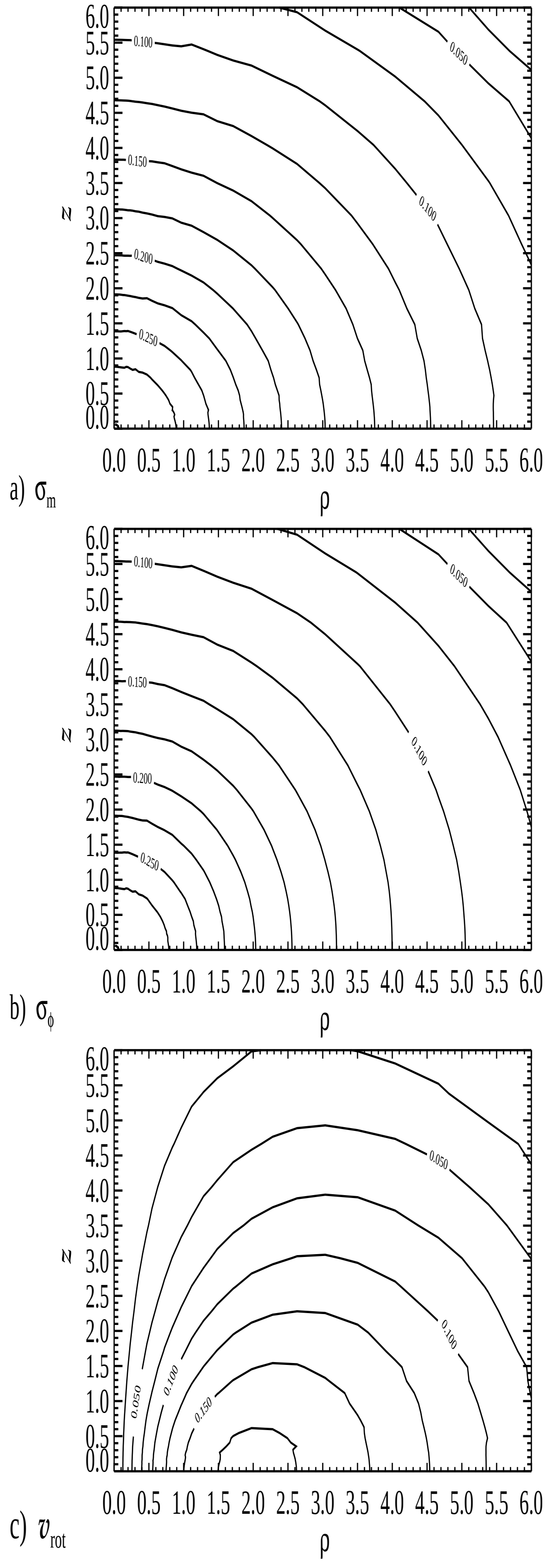

Figure 10. Contour maps a) of velocity dispersion in the meridional plane b) of the velocity dispersion in azimuthal direction and c) the rotational velocity for a model with $W_0 = 6$, $\omega_0 = 0.6$ and $t = \tau_{rh_0}$.

tours when the rotational velocity map is considered. Note, that the axes are measured in units of initial core radii and that the current core radius has already decreased to about $0.44\ r_{c_i}$.

5 SUMMARY AND DISCUSSION

We have performed 2D-Fokker-Planck simulations modelling the evolution of rotating stellar systems. The main results can be summarized as follows: large amounts of initial rotation drive the system into a phase of strong mass loss while it contracts slightly. The core is rotating even faster than before although angular momentum is transported outwards. At the same time the core is heating. Given these features we associate this phase with the gravo-gyro phase found by Hachisu (1979). The total collapse time is shortened appreciably by this effect, but the increase in central angular momentum levels off after about $2-3\ t_{r_h,i}$ indicating that the source of this 'catastrophe' ceases, i.e. it is not really a catastophe. Finally, the central angular velocity increases again, but with a rather small power of the central density – nearly the same power as for the central velocity dispersion during self-similar contraction. We propose to search for a self-similar solution of rotating cluster models in the future, which should agree with our findings.

Due to the non-locality of relaxation, the processes of mass loss, angular momentum transport and gravo-gyro and gravothermal 'catastrophe' in our models are not easily disentangled and as well are not entirely the same as e.g. in rotating gas spheroids. Additionally, even in that case no theoretical formulation of the problem has been found, yet. The only theoretical investigations undertaken so far concern rotating gas cylinders (Inagaki & Hachisu 1978, Hachisu 1979) and rotating gas disks (Hachisu 1982). But the mechanisms taking place in our comparatively complicated structure of a slightly flattened spheroid may be identified by analogy with an idealized transition between the cylinder and disk configurations of Hachisu (1982). The mechanism of gravogyro 'catastrophe' had been introduced by Hachisu (1979) for rotating gas cylinders, but these models do not comprise gravothermal 'catastrophe' for reasons concerning the curvature of the metric configuration (Hachisu 1982). On the other hand the investigation of interactions between gravogyro and gravothermal processes may be accomplished by considering the disk configuration in which both processes are active. There, it is shown that those terms in the tensor, which describes the hydrostatic readjustment of the system to a variation, that denote a coupling of quantities (e.g. angular momentum with temperature) play an important role for further evolution, thereby, e.g., adjusting the gravogyro to the gravothermal contraction. Then, the time scale of evolution will be given just by the efficiency of heat transport.

The time needed to reach collapse for each model is consistent with the individual mass loss rate (see Fig. (6), which itself is connected with the amount of angular momentum transport due to viscosity. The larger the initial amount of rotation the stronger the mass loss (see Fig. 6). Contrary to the simple models of Agekian (1958) stellar escapers from the system reach their escape energy in encounters mostly inside or near the core.

Due to both features – the total time to reach collapse depends on the amount of mass loss induced by viscosity effects and the solution for the gravothermal collapse is only moderately modified by gravogyro effects – it may be concluded, that the gravogyro 'catastrophe' is coupled to the gravothermal contraction and therefore does not evolve on time scales of angular momentum transport (viscosity coefficient) but rather on time scales of heat transport. This is clearly indicated by the lack of an early, separate central contraction phase of Lagrangian radii (see Fig. (1)) as it seemed to be implied by the N-body simulations of Akiyama & Sugimoto (1989). Note, however, that they did not include a tidal boundary. On the other hand gravogyro effects influence cluster evolution indirectly by increasing the mass loss activity thereby reducing the total collapse time.

One of the main results of this work is that a cluster system presently comprised of nearly spherical clusters may have had a distribution of cluster ellipticities up to strongly flattened, rotating stellar systems. This raises question for the origin of globular clusters: the picture presented here would be fully consistent with a formation from (obviously significantly rotating) giant molecular cloud like structures, when comparing their mass and angular momentum content (Akiyama & Sugimoto 1989). Other mechanisms, which are still not in contradiction to our results, incorporate the formation of rotating globular clusters from previously existing binary clusters, which suffer a synchronization instability leading to a merger (Sugimoto & Makino 1989). It is found that employing this mechanism a maximum flattening $e \approx 0.3$ of the globular clusters can be explained. The advantage of this model is that it explains very well several features of the Magellanic Clouds globular cluster system. The stronger flattening of Magellanic Cloud clusters as compared to those of the galaxy is in the light of our simulations understandable as a consequence of their dynamical age. Another possible mechanism to form binary clusters is collapse from a shell (Theis 1996). The formation of (single) clusters from collapsing shells has been proposed by Brown *et al.* (1991, 1995).

The rotation curves decrease with time, as do the ellipticity profiles, but the relative shapes of the latter do not vary much. The maximum values of rotational velocity and ellipticity remain at about the half mass radius throughout the evolution. In accord with our results Gebhardt *et al.* (1995) observe in 47Tuc by using non-parametric techniques an increase in the rotational velocity towards the half-mass radius and nearly solid body rotation inside the core. However, using the rotational velocity derived from integrated light (Gebhardt *et al.* 1994) they obtain an increasing angular velocity for the region inside half a core radius. Moreover, 47 Tuc reveals an already advanced stage of evolution, so that the results presented here indicate that a maximum in the velocity curve occurs at tens of current core radii (preliminary modelling gave about $20r_c(t)$ for a 47 Tuc - like model cluster). While the first argument may be reconciled with the results presented here (solid body rotation in the core and a rotation velocity peak at about the half-mass radius, which is roughly 10 core radii in the case of 47Tuc), when the bad statistics of the data beyond $\approx 2r_c$ in the observations are considered, the rise in angular velocity in the innermost central parts of the core, which are indicated by those observations may not be explained by our actual single mass models. There are several possible reasons, why our models may not yet be appropiate for 47Tuc: i) in 47Tuc as in any other cluster near core bounce there is significant activity of hard binaries going on, whose reaction products have been observed (Meylan *et al.* 1991); the present models do not yet incorporate binary energy generation; ii) the cluster mass function is observed to vary with radius and time both in spherical models and observations. Models including mass segregation effects may differ significantly from the single-mass case, as it is known for non-rotating clusters. For example it may be speculated that in deep core collapse high mass stars, which quickly segregate towards the centre, cannot loose angular momentum as efficiently as the stars in our simple models with equal masses do. iii) Finally, due to its very peculiar structure 47Tuc could be a non-axisymmetric cluster due to a recent encounter with the galactic disk, bulge or other cluster.

Future work, which will be published in the next papers of this series, consists of the incorporation of an energy source due to formation and hardening of three-body binaries (Bettwieser & Sugimoto 1984, Heggie & Ramamani 1989, Lee, Fahlman & Richer 1991) in order to proceed into the post-collapse phase, and the yet completely uninvestigated influence of differently rotating mass groups. Mass segregation would presumably alter the efficiency of angular momentum transport significantly. Such models will allow more detailed modelling of observed clusters, such as 47 Tuc or others.

Also it is important to consider the effects of different tidal boundary conditions and the dynamical influence of mass loss due to stellar evolution, both of which can alter the cluster structure considerably. As for the treatment of the tidal boundary it affects e.g. the anisotropy profile near the boundary. Drukier's (1995) boundary formulation with delayed mass loss beyond the tidal boundary, respectively, are worth trying out in this context. Finally, since the gravogyro contraction seems to take place in the very early evolution of the cluster, different initial conditions also may have important bearings on the rotational structure of the system.

We stress the necessity to perform N-body simulations of rotating systems in order to indicate the correctness of the assumptions made in the present Fokker-Planck models, especially to see the effects due to the neglect of the third integral.

ACKNOWLEDGMENTS

We wish to thank D. C. Heggie for kind hospitality during research visits in Edinburgh and for many interesting discussions as well as helpful comments and suggestions. Moreover, it is a pleasure for both authors to thank K. Takahashi and S. Inagaki for several fruitful discussions and kind hospitality during visits in Japan. The results presented are obtained in partial fulfillment of the Ph.D. requirements (C.E.) at Kiel University. This work was supported by DFG-grants Sp345/3-1 and /3-2 including a supplementary SPARCstation. C.E. is also grateful for support under the German-Japanese DFG-JSPS program (S. White, K. Nomoto) grant no. 446 JAP 113/109/0. Support for computing and visiting was provided by EPCC-staff, Edinburgh, in the frame of the TRACS scheme.

REFERENCES

Aarseth S. J., Hénon M., Wielen R., 1974, A&A, 37, 183
Agekian T. A., 1958, Soviet Astronomy AJ, 2, 22
Akiyama K., Sugimoto D., 1989, PASJ, 41, 991
Bettwieser E., Sugimoto D., 1984, MNRAS, 208, 439
Binney J. J., 1978, MNRAS, 183, 501
Brown J. H., Burkert A., Truran J. W., 1991, ApJ, 376, 115
Brown J. H., Burkert A., Truran J. W., 1995, ApJ, 440, 666
Chang J. S., Cooper G., 1970, J. Comp. Phys., 6, 1
Chernoff D. F., Weinberg M. D., 1990, ApJ, 351, 121
Cohn H., 1979, ApJ, 234, 1036
Cohn H., 1980, ApJ, 242, 765
Davoust E., Prugniel P., 1990, A&A, 230, 67
Drukier G., 1995, ApJS, 100, 347
Einsel Ch., Spurzem R., 1994, A. G. Abstr. Ser., 10, 185
Frenk C.S., Fall S.M., 1982, MNRAS, 199, 565
Fukushige T., Heggie D. C., 1995, MNRAS, 351, 121
Gebhardt K., Pryor C., Williams T. B., Hesser J. E., 1994, AJ, 107, 2067
Gebhardt K., Pryor C., Williams T. B., Hesser J. E., 1995, AJ, 110, 1699
Geyer E. H., Hopp U., Nelles B., 1983, A&A, 125, 359
Geyer E. H., Richtler T., 1982, Proc. IAU Colloq., 68, eds. Philip D., Hayes D. S., L. Davis Press, Schenectady
Giersz M., 1996, in "'Dynamical evolution of star clusters"', IAU Symp. No. 174, eds. P. Hut, J. Makino, Kluwer, Dordrecht, p. 101
Giersz M., Heggie D. C., 1994, MNRAS, 268, 257
Giersz M., Heggie D. C., 1994, MNRAS, 270, 298
Giersz M., Heggie D. C., 1996, MNRAS, 279,1037
Giersz M., Heggie D. C., 1997, MNRAS, in press
Giersz M., Spurzem R., 1994, MNRAS, 269, 241
Goodman J. J., 1983, Ph.D.-thesis, Princeton University
Hachisu I., 1979, PASJ, 31, 523
Hachisu I., 1982, PASJ, 34, 313
Heggie D. C., 1996, in "'Dynamical evolution of star clusters"', IAU Symp. No. 174, eds. P. Hut, J. Makino, Kluwer, Dordrecht, p. 131
Heggie D. C., Ramamani N., 1989, MNRAS, 237, 757
Henyey G. R., Wilets L., Böhm K. H., Le Levier R., Levee R. D., 1959, ApJ, 129, 628
Hut P., 1996, in "'Dynamical evolution of star clusters"', IAU Symp. No. 174, eds. P. Hut, J. Makino, Kluwer, Dordrecht, p. 121
Inagaki S., Hachisu, I., 1978, PASJ 30, 39
Kontizas E., Kontizas M., Sedmak G., Smareglia R., Dapergolas A., 1990, AJ, 100, 425
Lee H. M., Fahlman G. G., Richer H. B., 1991, ApJ, 366, 455
Longaretti P.-Y., Lagoute C., 1996, A&A, 308, 453
Louis P. D., Spurzem R., 1991, MNRAS, 251, 408
Lupton R. H., Gunn J. E., 1987, AJ, 93, 1106
Lynden-Bell D., Eggleton P. P., 1980, MNRAS, 191, 483
Lynden-Bell D., Wood R., 1968, MNRAS, 138, 495
Meylan G., Dubath P., Mayor M., 1991, A&A, 383, 587
Meylan G., Mayor M., 1986, A&A, 166, 122
Merritt D., Meylan G., Mayor M., 1997, ApJ, submitted
Murphy B. W., Cohn H., Hut P., 1990, MNRAS, 245, 335
Quinlan G. D., 1996, New Astronomy, 1, 255
Pease F. G., Shapley H., 1917, Contr. Mt. Wilson Obs., 129
Rosenbluth M. N., MacDonald W. M., Judd D. L., 1957, Phys.Rev., 107, 1
Spitzer L., 1987, "'Dynamical evolution of globular clusters"', Princeton Univ. press
Spitzer L., Hart M. H., 1971, ApJ, 164, 399
Spurzem R., 1994, in "'Ergodic concepts in stellar dynamics"', eds. D. Pfenniger, V. Gurzadyan, Springer-Verlag, Berlin, p.170
Spurzem R., 1996, in "'Dynamical evolution of star clusters"', IAU Symp. No. 174, eds. P. Hut, J. Makino, Kluwer, Dordrecht, p.111
Staneva A., Spassova N., Golev V., 1996, A&AS, 116, 447
Sugimoto D., Makino J., 1989, PASJ, 41, 1117
Takahashi K., 1996, PASJ, 47, 561
Takahashi K., 1996, PASJ, 48, 691
Theis C., 1996, in "'Dynamical evolution of star clusters"', IAU Symp. No. 174, eds. P. Hut, J. Makino, Kluwer, Dordrecht, p. 399
White E. R., Shawl J. S., 1987, ApJ, 317, 246

APPENDIX A: DERIVATION OF THE FLUX COEFFICIENTS

When deriving diffusion coefficients several ways may be chosen for doing it. We decided to follow the approach of Rosenbluth, MacDonald & Judd (1957) involving covariant derivatives of tensorial objects. At first, the coordinate systems will be introduced. While we have cylindrical coordinates in coordinate space (ρ, z, φ), the following symmetry is applied to velocity space: $q^1 = v = (v_\rho^2 + v_\varphi^2 + v_z^2)^{\frac{1}{2}}$; $q^2 = \psi = \arctan(v_\rho/v_z)$; $q^3 = v_\varphi$, where (v_ρ, v_φ, v_z) are local cartesian velocity coordinates. The corresponding metric tensor $(a^{\mu\nu})$ then reads as

$$a^{\mu\nu} = \begin{pmatrix} 1 & 0 & \frac{v_\varphi}{v} \\ 0 & \frac{1}{(v_\rho^2+v_z^2)} & 0 \\ \frac{v_\varphi}{v} & 0 & 1 \end{pmatrix} \tag{A1}$$

with the volume element $a := \det(a_{\mu\nu}) = 1/\det(a^{\mu\nu}) = v^2$. The tensorial form of the Fokker-Planck equation may generally be written as

$$\frac{1}{\Gamma_a}\frac{\partial f_a}{\partial t} = -(fT_a^\mu)_{,\mu} + \frac{1}{2}(fS_a^{\mu\nu})_{,\mu\nu}\,, \tag{A2}$$

where the commas denote covariant derivatives, and the subscript a indicates particle species. The factor $\Gamma_a = 4\pi G m_a^2 \ln\Lambda$ contains the usual Coulomb logarythm. The diffusion coefficients of Cartesian coordinate systems may then be expressed as tensorial objects

$$\frac{1}{\Gamma_a} < \Delta v^\mu >_a = T_a^\mu = a^{\mu\nu}(h_a)_{,\nu} \tag{A3}$$

$$\frac{1}{\Gamma_a} < \Delta v^\mu \Delta v^\nu >_a = S^{\mu\nu} = a^{\mu\omega}a^{\nu\tau}(g)_{,\omega\tau}\,. \tag{A4}$$

The functions h and g are the so called Rosenbluth potentials:

$$h_a(\vec{v}) = \Sigma_b \frac{m_a + m_b}{m_b}\int d\vec{v}'_f f_b(\vec{v}'_f)\frac{1}{\left|\vec{v} - \vec{v}'_f\right|} \tag{A5}$$

$$g(\vec{v}) = \Sigma_b \int d\vec{v}'_f f_b(\vec{v}'_f)\left|\vec{v} - \vec{v}'_f\right| \tag{A6}$$

After some lengthy calculations involving Christoffel symbols we arrive at the following expressions for the tensors given above (note, that symmetry is assumed about ψ):

$$T_a^1 = \frac{\partial h}{\partial v} + \frac{v_\varphi}{v}\frac{\partial h}{\partial v_\varphi} \tag{A7}$$

$$T_a^2 = 0 \tag{A8}$$

$$T_a^3 = \frac{v_\varphi}{v}\frac{\partial h}{\partial v} + \frac{\partial h}{\partial v_\varphi} \tag{A9}$$

$$S^{11} = \frac{\partial^2 g}{\partial v^2} + 2\frac{v_\varphi}{v}\frac{\partial^2 g}{\partial v \partial v_\varphi} + \frac{v_\varphi^2}{v^2}\frac{\partial^2 g}{\partial v_\varphi^2} \tag{A10}$$

$$S^{12} = S^{21} = 0 \tag{A11}$$

$$S^{13} = S^{31} = \frac{v_\varphi}{v}\frac{\partial^2 g}{\partial v^2} + (1 + \frac{v_\varphi^2}{v^2})\frac{\partial^2 g}{\partial v \partial v_\varphi} + \frac{v_\varphi}{v}\frac{\partial^2 g}{\partial v_\varphi^2} \tag{A12}$$

$$S^{22} = \frac{1}{v(v^2 - v_\varphi^2)}\frac{\partial g}{\partial v} \tag{A13}$$

$$S^{23} = S^{32} = 0 \tag{A14}$$

$$S^{33} = \frac{v_\varphi^2}{v^2}\frac{\partial^2 g}{\partial v^2} + \frac{\partial^2 g}{\partial v_\varphi^2} + \frac{(v^2 - v_\varphi^2)}{v^3}\frac{\partial g}{\partial v} + 2\frac{v_\varphi}{v}\frac{\partial^2 g}{\partial v_\varphi^2} \tag{A15}$$

Thus, employing the relations

$$(fT_a^\mu)_{,\mu} = \sqrt{a}^{-1}\frac{\partial}{\partial q^\mu}\left(\sqrt{a} f T_a^\mu)\right) \tag{A16}$$

$$\begin{aligned}(fS_a^{\mu\nu})_{,\mu\nu} &= \sqrt{a}^{-1}\tfrac{\partial^2}{\partial q^\mu \partial q^\nu}\left(\sqrt{a} f S^{\mu\nu}\right) \\ &\quad + \sqrt{a}^{-1}\tfrac{\partial}{\partial q^\nu}\left(\sqrt{a}\Gamma^\nu_{\omega\mu} f S^{\mu\omega}\right)\end{aligned} \tag{A17}$$

with the Γ symbol denoting a Christoffel symbol of the second kind, here, the Fokker-Planck equation consists of terms

$$\begin{aligned}(fT_a^\mu)_{,\mu} &= \frac{1}{v}\left(\frac{\partial}{\partial v}\left(vf\frac{\partial h}{\partial v} + v_\varphi f\frac{\partial h}{\partial v_\varphi}\right)\right. \\ &\quad \left. + \frac{\partial}{\partial v_\varphi}\left(v_\varphi f\frac{\partial h}{\partial v} + vf\frac{\partial h}{\partial v_\varphi}\right)\right)\end{aligned} \tag{A18}$$

and

$$\begin{aligned}(fS_a^{\mu\nu})_{,\mu\nu} &= \frac{1}{v}\left\{\frac{\partial^2 g}{\partial v^2}\left(vfS_a^{11}\right) + 2\frac{\partial^2 g}{\partial v \partial v_\varphi}\left(vfS_a^{13}\right)\right. \\ &\quad \left. + \frac{\partial^2 g}{\partial v_\varphi^2}\left(vfS_a^{33}\right)\right\} \\ &\quad + \frac{1}{v}\left\{\frac{\partial}{\partial v}\left(vf\left[\frac{-(v^2 - v_\varphi^2)}{v^3}\frac{\partial^2 g}{\partial v_\varphi^2}\right.\right.\right. \\ &\quad \left.\left.\left. - \frac{2}{v^2}\frac{\partial g}{\partial v}\right]\right)\right\} .\end{aligned} \tag{A19}$$

Most terms involving S^{22} vanisch due to further derivations with respect to the coordinate of symmetry, ψ, but one of them is retained in the last term in Eq. (A19), therein written explicitly. The diffusion coefficients in transformations between curvilinear coordinate systems may now be identified using

$$\frac{1}{\Gamma_a} < \Delta v^\mu >_a = T_a^\mu - \frac{1}{2}\Gamma^\mu_{\omega\tau} S^{\omega\tau} \tag{A20}$$

$$\frac{1}{\Gamma_a} < \Delta v^\mu \Delta v^\nu > = S_a^{\mu\nu} , \tag{A21}$$

where the additional term in Eq. (A20) with respect to the case of Eq. (A3) originates from the second (last) term of Eq. (A19).

It is convenient to treat the problem in energy - angular momentum - space such that the diffusion coefficients just derived have to be transformed to the new velocity variables $E = \frac{1}{2}v^2 + \Phi(\rho, z)$ and $J_z = \rho v_\varphi$. This can be accomplished by using the following simple formula:

$$< \Delta E > = E_{,\mu} < \Delta v^\mu > + \frac{1}{2}E_{,\mu\nu} < \Delta v^\mu \Delta v^\nu > \tag{A22}$$

$$< \Delta J_z > = J_{,\mu} < \Delta v^\mu > + \frac{1}{2}J_{,\mu\nu} < \Delta v^\mu \Delta v^\nu > \tag{A23}$$

$$< (\Delta E)^2 > = E_{,\mu} E_{,\nu} < \Delta v^\mu \Delta v^\nu > \tag{A24}$$

$$< (\Delta J_z)^2 > = J_{,\mu} J_{,\nu} < \Delta v^\mu \Delta v^\nu > \tag{A25}$$

$$< \Delta E \Delta J_z > = E_{,\mu} J_{,\nu} < \Delta v^\mu \Delta v^\nu > \tag{A26}$$

If we now assume an isotropic background distribution $f(v_f)$, integrals h and g are easily simplified (*cf.* Spitzer 1987, p.36). For this purpose, we express the velocity $\vec{v}$ (inertial frame) in terms of velocities ($\vec{u} + \rho\Omega\vec{e_\varphi}$) in the corotating frame. Ω is the angular velocity of the corotating frame. Thus, $f(u)$ is isotropic and the derivatives of h and g with respect to v and v_φ ($\frac{\partial h}{\partial v}$, $\frac{\partial h}{\partial v_\varphi}$, etc.) must be transformed to those with respect to u only. For example, $\frac{\partial h}{\partial v_\varphi} = -\frac{\rho\Omega}{u}\frac{\partial h}{\partial u}$. Inserting eqs. (A7) to (A15) in eqs. (A20), (A21) and employing these results again in eqs. (A22...A26) under consideration of the transformation to the corotating frame, we arrive at

$$\begin{aligned}< \Delta E > &= \left(u + \frac{J_z\Omega}{u} - \frac{\rho^2\Omega^2}{u}\right)\frac{\partial h}{\partial u} \\ &\quad + \frac{1}{2}\frac{\partial^2 g}{\partial u^2} \\ &\quad + \frac{1}{u}\frac{\partial g}{\partial u} ,\end{aligned} \tag{A27}$$

$$< \Delta J_z > = \left(\frac{J_z}{u} - \frac{\rho^2\Omega}{u}\right)\frac{\partial h}{\partial u} , \tag{A28}$$

$$\begin{aligned}< (\Delta E)^2 > &= \left(u^2 + 2J_z\Omega - 2\rho^2\Omega^2 + \frac{J_z^2\Omega^2}{u^2}\right. \\ &\quad \left. - \frac{2J_z\rho^2\Omega^3}{u^2} + \frac{\rho^4\Omega^4}{u^2}\right)\frac{\partial^2 g}{\partial u^2} \\ &\quad + \left(\frac{\rho^2\Omega^2}{u} - \frac{J_z^2\Omega^2}{u^3}\right. \\ &\quad \left. + \frac{2J_z\rho^2\Omega^3}{u^3} - \frac{\rho^4\Omega^4}{u^3}\right)\frac{\partial g}{\partial u} ,\end{aligned} \tag{A29}$$

$$\begin{aligned}< (\Delta J_z)^2 > &= \left(\frac{J_z^2}{u^2} + \frac{\rho^4\Omega^2}{u^2} - \frac{2J_z\rho^2\Omega}{u^2}\right)\frac{\partial^2 g}{\partial u^2} \\ &\quad + \left(\frac{-J_z^2}{u^3} - \frac{\rho^4\Omega^2}{u^3}\right. \\ &\quad \left. + \frac{\rho^2}{u} + \frac{2J_z\rho^2\Omega}{u^3}\right)\frac{\partial g}{\partial u} ,\end{aligned} \tag{A30}$$

$$< \Delta E \Delta J_z > = \left(J_z - \rho^2\Omega + \frac{J_z^2\Omega}{u^2} - \frac{2J_z\rho^2\Omega^2}{u^2} + \frac{\rho^4\Omega^3}{u^2} \right) \frac{\partial^2 g}{\partial u^2} + \left(\frac{\rho^2\Omega}{u} + \frac{2J_z\rho^2\Omega^2}{u^3} - \frac{J_z^2\Omega}{u^3} - \frac{\rho^4\Omega^3}{u^3} \right) \frac{\partial g}{\partial u} , \tag{A31}$$

The Fokker-Planck equation is usually recast in flux conservation form:

$$\frac{Df}{Dt} = -\frac{\partial F_E}{\partial E} - \frac{\partial F_{J_z}}{\partial J_z}, \tag{A32}$$

where we still have not applied an orbit average. The term on the left hand side represents the Vlasov-term of the full collisional Boltzmann equation. The fluxes F are given by

$$F_E = -D_{EE}\frac{\partial f}{\partial E} - D_{EJ_z}\frac{\partial f}{\partial J_z} - D_E f \tag{A33}$$

$$F_{J_z} = -D_{J_zJ_z}\frac{\partial f}{\partial J_z} - D_{J_zE}\frac{\partial f}{\partial E} - D_{J_z} f. \tag{A34}$$

Comparing eqs. (A32 - A34) with the original form (e.g. Spitzer 1987) the flux coefficients D may be identified to

$$\begin{aligned} D_{EE} &= \tfrac{1}{2} < (\Delta E)^2 > \\ D_{EJ_z} &= \tfrac{1}{2} < \Delta E \Delta J_z > \\ D_{J_zJ_z} &= \tfrac{1}{2} < (\Delta J_z)^2 > \\ D_{JE_z} &= \tfrac{1}{2} < \Delta E \Delta J_z > \\ D_E &= - < \Delta E > + \tfrac{1}{2}\tfrac{\partial}{\partial E} < (\Delta E)^2 > \\ &\quad + \tfrac{1}{2}\tfrac{\partial}{\partial J_z} < \Delta E \Delta J_z > \\ D_{J_z} &= - < \Delta J_z > + \tfrac{1}{2}\tfrac{\partial}{\partial J_z} < (\Delta J_z)^2 > \\ &\quad + \tfrac{1}{2}\tfrac{\partial}{\partial E} < \Delta E \Delta J_z > \end{aligned} \tag{A35}$$

Inserting the expressions for the diffusion coefficients given above, one obtains finally the desired flux coefficients for the axially symmetric application with rotation. We find

$$D_E = 4\pi \left(\frac{J_z\Omega}{u} - \frac{\rho^2\Omega^2}{u} + u \right) F_2(u), \tag{A36}$$

$$D_{J_z} = 4\pi \left(\frac{J_z}{u} - \frac{\rho^2\Omega}{u} \right) F_2(u), \tag{A37}$$

$$\begin{aligned} D_{EE} &= \frac{4\pi}{3}\left(2uJ_z\Omega - u\rho^2\Omega^2 + u^3\right) E_1(u) \\ &+ 2\pi \left(u\rho^2\Omega^2 - \frac{J_z^2\Omega^2}{u} + \frac{2J_z\rho^2\Omega^3}{u} - \frac{\rho^4\Omega^4}{u} \right) F_2(u) \\ &+ 2\pi \left(\frac{2u^3}{3} + \frac{4}{3}uJ_{z\rho} - \frac{5}{3}u\rho^2\Omega^2 + \frac{J_z^2\Omega^2}{u} + \frac{\rho^4\Omega^4}{u} \right) F_4(u) , \end{aligned} \tag{A38}$$

$$\begin{aligned} D_{J_zJ_z} &= \frac{4\pi}{3}u\rho^2 E_1(u) \\ &+ 2\pi \left(u\rho^2 - \frac{J_z^2}{u} - \frac{\rho^4\Omega^2}{u} + \frac{2J_z\rho^2\Omega}{u} \right) F_2(u) \\ &\quad 2\pi \left(\frac{J_z^2}{u} + \frac{\rho^4\Omega^2}{u} - \frac{2J_z\rho^2\Omega}{u} - \frac{1}{3}u\rho^2 \right) F_4(u) . \end{aligned} \tag{A39}$$

$$\begin{aligned} D_{EJ_z} &= \frac{4\pi}{3}uJ_zE_1(u) \\ &+ 2\pi \left(u\rho^2\Omega + \frac{2J_z\rho^2\Omega^2}{u} - \frac{J_z^2\Omega}{u} - \frac{\rho^4\Omega^3}{u} \right) F_2(u) \\ &+ 2\pi \left(\frac{2}{3}uJ_z - u\rho^2\Omega - \frac{2J_z\rho^2\Omega^2}{u} + \frac{\rho^4\Omega^3}{u} + \frac{J_z^2\Omega}{u} \right) F_4(u) . \end{aligned} \tag{A40}$$

The functions E_i and F_i are constituent parts of the Rosenbluth potentials and their derivatives.

$$F_i = \frac{1}{u^i}\int_0^u u'^i f(u')du' \tag{A41}$$

$$E_i = \frac{1}{u^i}\int_u^\infty u'^i f(u')du' \tag{A42}$$

Given an expression for the background distribution function (section 2, rotating King-model used throughout this paper) these functions are evaluated for each position in the meridional plane, when the local density, mean particle velocity and mean particle angular velocity are specified.

The next step is to orbit average these flux coefficients and again to transform them to (X, Y)-coordinates used throughout our numerical simulations.